Analog CMOS Implementation of a CNN-Based Locomotion Controller With Floating-Gate Devices

Kazuki Nakada, *Associate Member, IEEE*, Tetsuya Asai, *Member, IEEE*, and Yoshihito Amemiya

***Abstract*—This paper proposes an analog CMOS circuit that implements a central pattern generator (CPG) for locomotion control in a quadruped walking robot. Our circuit is based on an affine transformation of a reaction-diffusion cellular neural network (CNN), and uses differential pairs with multiple-input floating-gate (MIFG) MOS transistors to implement both the nonlinearity and summation of CNN cells. As a result, the circuit operates in voltage mode, and thus it is expected to reduce power consumption. Due to good matching accuracy of devices, the circuit generates stable rhythmic patterns for robot locomotion control. From experimental results on fabricated chip using a standard CMOS 1.5-μm process, we show that the chip yields the desired results; i.e., stable rhythmic pattern generation and low power consumption.**

***Index Terms*—Analog CMOS circuit, biologically-inspired robotics, cellular neural network, central pattern generator, multiple-input floating-gate MOS FETs.**

I. Introduction

CONTROLLING walking machines is a difficult task that requires the coordination of physical parts with multiple degrees of freedom. Currently, scientific interest increasingly has focused on biological systems that control complicated multiple joints and muscles during locomotion, such as walking, running, swimming and flying. Biological systems have evolved and optimized themselves under selective pressures, and therefore we expect that such systems will provide us with valuable insights into solving these tasks. In fact, biological findings have suggested that there are universal principles that cut across a wide variety of animals, and these offer ideas for designing and controlling robots [1].

Central pattern generators (CPGs) [2] are biological neural networks that generate fundamental rhythmic movements for locomotion of animals. Such rhythmic movements induce coordination in physical parts, resulting in stable locomotion. While it is not necessary to generate rhythmic pattern for locomotion, sensory feedback modulates CPG activities to adapt to varying situations [3]. Furthermore, CPG can change the locomotion pattern itself. For instance, horses select an optimal locomotion pattern, such as walk, trot and gallop, depending on the given situation [4].

Manuscript received April 6, 2004; revised September 1, 2004. This paper was recommended by Associate Editor B. Shi.

The authors are with the Department of Electrical Engineering, Hokkaido University, Sapporo 060-8628, Japan (e-mail: nakada@sapiens-ei.eng.hokudai.ac.jp).

Digital Object Identifier 10.1109/TCSI.2005.849120

During the past decade, many researchers have designed and implemented locomotion controllers based on the CPG framework in robotics, focusing on such CPG functions [11]–[17]. These CPG controllers have advantages in: 1) reducing the amount of calculation required to control locomotion because there is no need for complicated planning to generate motion trajectories and 2) high adaptation to unexpected disturbances as a result of a CPG interacting with the environment through sensory information.

Recently, Arena *et al.* have applied a class of cellular neural networks (CNNs) as CPG controllers to biologically-inspired robots [31], [32]. In general, a CNN is an analog dynamic processor array with local connections, and it can thus essentially do parallel and distributed processing, and continuous time and value signal processing [22]–[24]. In addition, their CNN is a class of autonomous CNNs that can generate various spatial-temporal patterns automatically [25]–[29]. Therefore, it is suitable to use as an artificial CPG controller to generate rhythmic motion patterns for robotic locomotion in real time.

In this paper, we propose an analog CMOS chip that implements a class of CNNs to control locomotion in quadruped walking robots. CNN-based CPG controllers have already been implemented on silicon chips [20], [21]. In these chips, the components called cells interact with neighboring ones through current, and thus these chips have problems in terms of current mismatch and power consumption. The power consumption is a particularly critical problem in long term operation. Hence, we introduced an affine transformation of a reaction-diffusion CNN, and designed it as an analog CMOS circuit using differential pairs with multiple-input floating-gate (MIFG) MOS transistors [35], [36], aimed at implementing the nonlinearity and summation in CNN cells. As a result, the CNN circuit operates in voltage-mode, and it is thus expected to reduce bias currents and the total amount of power consumption. Furthermore, the circuit is expected to operate accurately due to good matching accuracy of devices. We fabricated an experimental chip using a standard CMOS process. From results on the fabricated chip, we show that the chip generates stable rhythmic patterns to control robotic locomotion under an actual environment, and consumes low electrical power.

This paper is organized as follows. In Section II, we propose a novel CNN-based CPG model for constructing a locomotion controller. In Section III, we describe an analog CMOS implementation of the CNN-based CPG model. In Section IV, we present the measured results obtained from the experimental chip. We discuss the advantages and the disadvantages of our chip in Section V. The summary over the present research is presented in Section IV.

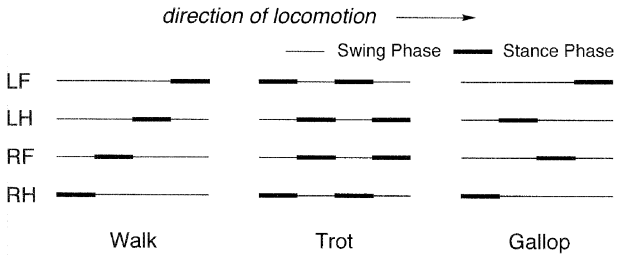

Fig. 1. Typical locomotion patterns of mammals, such as walk, trot, and gallop, in which bold lines and thin lines represent stance and swing phase.

II. CNN-Based Central Pattern Generator

We here propose a novel CNN-based CPG model that enables interlimb coordination in a quadruped walking robot.

A. Central Pattern Generator

Let us briefly review the biological principles in locomotion control of animals. Locomotion of animals, such as walking, running, swimming, and flying, is based on rhythmic movements, which are generated by a biological neural network known as CPG [2]. CPG consists of sets of neural oscillators, situated in the ganglion or the spinal cord. Induced by inputs from higher level, a CPG generates a rhythmic pattern of neural activity automatically. This rhythmic pattern activating the motor neurons induces rhythmic movements of animals. While not necessary for generating the rhythmic movement itself, sensory feedback modulates the frequency and phase of the rhythmic pattern generated by CPG. Consequently, CPG adapts itself to varying situations [3].

One of the most fundamental functions of CPG is to control individual limbs. As a result of interacting with CPGs that actuate muscles at each joint of limbs, rhythmic movements in the individual limbs are stabilized. Another is cooperation between limbs, i.e., interlimb coordination. CPGs that control each of the limbs are synchronized via their coordinating interneurons, and thus interlimb coordination is achieved. Since the degrees of freedom of physical parts relevant to locomotion are very high, the coordination of physical parts, such as interlimb coordination, is necessary for stable locomotion [3].

In locomotion of animals, different patterns of interlimb coordination, called the gait, can be observed. The observed gait is characterized by a phase relationship in limb movements. Fig. 1 has phase diagrams of typical gait patterns in mammals, such as the walk, trot and gallop. Here, LF, LH, RF, and RH represent the left forelimb, left hindlimb, right forelimb, and right hindlimb. During locomotion, one cycle of each limb movement is divided into two phases, i.e., stance and swing phase. In the stance phase, each limb is placed on the ground. In the swing phase, each limb acts as a pendulum swing by muscles and gravity. Each gait is also considered as the phase-locked oscillation of limbs. It is believed that vertebrates, such as horses and cats, select an optimal gait pattern depending on the given situation as a result of the changing cooperation of CPGs that control interlimb coordination [4].

B. CNN-Based CPG Model for Interlimb Coordination

We here propose a CPG model that underlies the locomotion controller to achieve interlimb coordination in a quadruped walking robot. Many CPG models have been proposed in previous works (e.g., [7]–[10]). Most have been constructed using coupled nonlinear oscillators, each actuating the joints of the limb.

Arena *et al.* proposed a class of CNNs as the CPG model to control locomotion in biologically-inspired robots, such as in a hexapod robot and a sea-lamprey robot [31], [32]. Their model can be represented by the following:

$$\dot{x}^1_{i,j} = -x^1_{i,j} + (1+\mu)y^1_{i,j} - sy^2_{i,j} + S^1_{i,j} \quad (1)$$

$$\dot{x}^2_{i,j} = -x^2_{i,j} + sy^1_{i,j} + (1+\mu)y^2_{i,j} + S^2_{i,j} \quad (2)$$

and

$$S^1_{i,j} = D_1(y^1_{i-1,j}+y^1_{i+1,j}+y^1_{i,j-1}+y^1_{i,j+1}-4y^1_{i,j}) + I^1_{i,j} \quad (3)$$

$$S^2_{i,j} = D_2(y^2_{i-1,j}+y^2_{i+1,j}+y^2_{i,j-1}+y^2_{i,j+1}-4y^2_{i,j}) + I^2_{i,j} \quad (4)$$

where $x^n_{i,j}$ represent a state variable, $I^n_{i,j}$ a bias constant, (i,j) is a grid point in the cell. Here, μ and s are coupling parameters, D_n a diffusive coefficient, and output $y^n_{i,j} = f(x^n_{i,j})$, $(n = 1, 2)$, which is a nonlinear function usually given by the piecewise linear function or the sigmoid function.

This model was originally proposed as the reaction-diffusion (RD) CNN to simulate RD partial differential equations. [30]. The RD-CNN is a class of autonomous CNNs that can produce various complex spatial-temporal patterns automatically [30], [31], and it is thus suitable for an artificial CPG to generate various rhythmic motion patterns to control robot locomotion.

Let us introduce a novel class of CNNs, which is suitable for implementing an analog CMOS circuit that operates in voltage-mode. Firstly, we rewrite (1)–(4) as follows:

$$\dot{x}^1_{i,j} = -x^1_{i,j} + \sum_{k,l} A_{i,j;k,l}y^1_{k,l} - \sum_{k,l} B_{i,j;k,l}y^2_{k,l} + I^1_{i,j} \quad (5)$$

$$\dot{x}^2_{i,j} = -x^2_{i,j} + \sum_{k,l} C_{i,j;k,l}y^1_{k,l} - \sum_{k,l} D_{i,j;k,l}y^2_{k,l} + I^2_{i,j} \quad (6)$$

where $A_{i,j;k,l}$, $B_{i,j;k,l}$, $C_{i,j;k,l}$ and $D_{i,j;k,l}$ represent coupling coefficients, and (k,l) is a grid point in the neighborhood of the point (i,j). The above formalism can naturally be extended to include the cross diffusion terms. We then rewrite these equations in terms of a new state variable $v^n_{i,j}$ as follows:

$$\dot{v}^1_{i,j} = -v^1_{i,j} + f\left(\sum_{k,l} A_{i,j;k,l}v^1_{k,l} - \sum_{k,l} B_{i,j;k,l}v^2_{k,l} + I^1_{i,j}\right) \quad (7)$$

$$\dot{v}^2_{i,j} = -v^2_{i,j} + f\left(\sum_{k,l} C_{i,j;k,l}v^1_{k,l} - \sum_{k,l} D_{i,j;k,l}v^2_{k,l} + I^2_{i,j}\right). \quad (8)$$

The equations can be derived from (5) and (6) by the following transformation:

$$x^1_{i,j} = \sum_{k,l} A_{i,j;k,l}v^1_{k,l} - \sum_{k,l} B_{i,j;k,l}v^2_{k,l} + I^1_{i,j} \quad (9)$$

$$x^2_{i,j} = \sum_{k,l} C_{i,j;k,l}v^1_{k,l} - \sum_{k,l} D_{i,j;k,l}v^2_{k,l} + I^2_{i,j}. \quad (10)$$

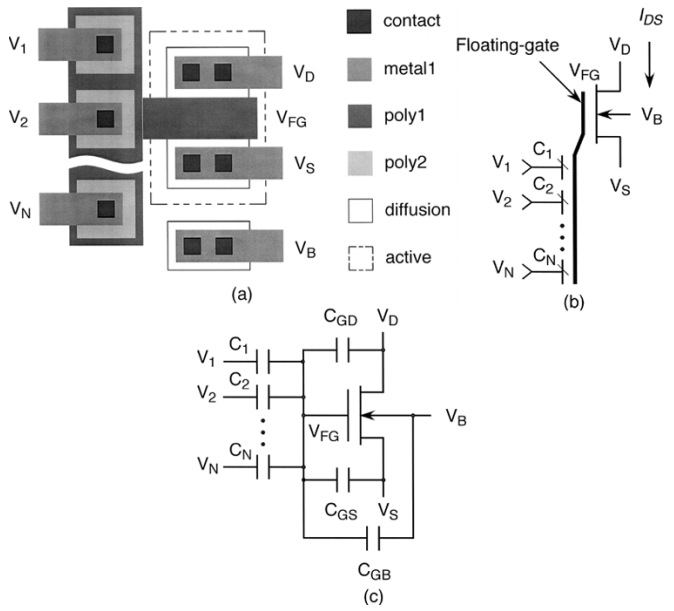

Fig. 2. Multiple-input floating-gate MOS transistor. (a) Chip layout. (b) Circuit symbol. (c) Equivalent circuit.

The transformation above is an Affine, and its inverse transformation is also an Affine. Thus, (5)–(6) and (7)–(8) are dynamically equivalent. In case of $f(x) = \tanh(x)$, the above transformation can similarly be checked. As it is shown in the following section in detail, the transformation is useful in chip implementation rather than as a mathematical problem. In addition, from the biological point of view, the above formalism is a special case of the Wilson-Cowan neural system [6] whose components are locally connected within their neighborhood. In the following, we are going to consider the transformed CNN equations given by (7)–(8) as a CPG model to do interlimb coordination in a quadruped walking robot.

III. Circuitry Architecture

We here describe the implementation of an analog CMOS circuit with the CNN-based CPG model.

A. Cell Circuit

First, we will describe a cell circuit that constitutes a part of the CNN circuit. The cell circuit consists of four analog elementary circuits, i.e., a differential pair, a current mirror, an RC circuit, and a current source.

The differential pair, the most fundamental components of the cell circuit, can approximate the sigmoidal function. In the following, we assumed that the MOS transistors comprising the differential pair operate in weak inversion (subthreshold) region, thereby, reducing current consumption. The static response of the differential pair is represented as [33]

$$I_\mu(V^+ - V^-) = I_b \frac{1 + \tanh(\mu(V^+ - V^-))}{2} \qquad (11)$$

where I_μ is the output current of the differential pair, V^+ and V^- the input voltages, I_b the bias current, $\mu = \kappa/2U_{\rm T}$, $U_{\rm T}$ the thermal voltage, and κ the effectiveness of the gate potential. By subtracting half the bias current from output current I_μ, the

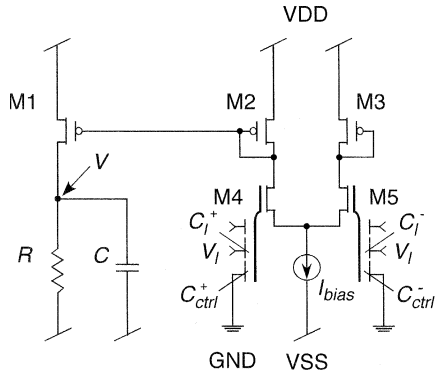

Fig. 3. Schematic of cell circuit.

characteristics of the nonlinear function $f(x)$, described in Section II, can be obtained.

We replace the MOS transistors in the differential pair with MIFG MOS transistors [35], [36] (Fig. 2), aiming at the operation of weighted linear summation of voltages. The floating-gate voltage of the transistor is expressed by the following [36]:

$$V_{\rm FG} = \frac{C_{\rm GD}}{C_{\rm T}} V_{\rm D} + \frac{C_{\rm GS}}{C_{\rm T}} V_{\rm S} + \frac{C_{\rm GB}}{C_{\rm T}} V_{\rm B} + \frac{Q_0}{C_{\rm T}} + \sum_l^N \frac{C_l}{C_{\rm T}} V_l \qquad (12)$$

where V_l is the lth input gate voltage, C_l the capacitance between each of the input gates and the floating-gate, $V_{\rm D}$, $V_{\rm S}$ and $V_{\rm B}$ the voltage of drain, source and bulk, Q_0 represents an initial charge in the floating-gate, and the total capacitance of the floating-gate is expressed by

$$C_{\rm T} = C_{\rm GD} + C_{\rm GS} + C_{\rm GB} + \sum_l^N C_l \qquad (13)$$

where $C_{\rm GD}$, $C_{\rm GS}$ and $C_{\rm GB}$ represent the capacitance between the floating-gate and drain, source and bulk, respectively. If the transistors in the differential pair are well matched, the effect of the charges in $C_{\rm GD}$, $C_{\rm GS}$ and $C_{\rm GB}$ can be cancelled. If we reduce Q_0 to zero, and then the differential voltages between the floating-gates of the transistors in the differential pair can approximately be expressed by the following:

$$V_{\rm FG}^+ - V_{\rm FG}^- \simeq \sum_l^N \frac{C_l^+}{C_{\rm T}} V_l^+ - \sum_l^N \frac{C_l^-}{C_{\rm T}} V_l^- \qquad (14)$$

where $V_{\rm FG}^+$ and $V_{\rm FG}^-$ are the floating-gate voltages, V_l^+ and V_l^- the input gate voltages, C_l^+ and C_l^- the capacitances between each of the input gates and the floating-gate.

Fig. 3 shows the schematic of the cell circuit. After the output current of the differential pair I_μ is reversed by current mirror, it is integrated by the RC circuit. The circuit dynamics are expressed by the following :

$$C\dot{V} = -\frac{V - {\rm VSS}}{R} + I_\mu(V_{\rm FG}^+ - V_{\rm FG}^-) \qquad (15)$$

where C is the capacitance, R the resistance, V the voltage across the RC circuit, which corresponds to a state variable, and VSS the substrate voltage. For purposes of setting the equilibrium voltage of the cell circuit at zero, we set ${\rm VSS} < 0$ and

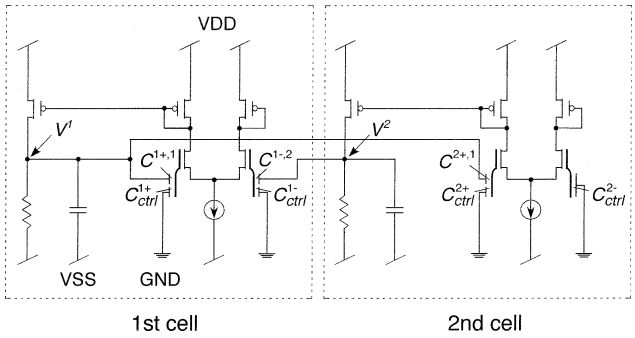

Fig. 4. Schematic of unit circuit.

$\mathrm{VSS}/R + I_b/2 = 0$. Then, the equation above can be rewritten as follows:

$$C\dot{V} = -\frac{V}{R} + \frac{I_b}{2}\tanh(\mu(V_{\mathrm{FG}}^{+} - V_{\mathrm{FG}}^{-})) \tag{16}$$

$$\simeq -\frac{V}{R} + \frac{I_b}{2}\tanh\left(\mu\left(\sum_l \frac{C_l^{+}}{C_{\mathrm{T}}}V_l^{+} - \sum_l \frac{C_l^{-}}{C_{\mathrm{T}}}V_l^{-}\right)\right) \tag{17}$$

$$= -\frac{V}{R} + \frac{I_b}{2}F_\mu\left(\sum_l C_l^{+}V_l^{+} - \sum_l C_l^{-}V_l^{-}\right) \tag{18}$$

where we have replaced $F_\mu(x) = \tanh(\mu x/C_{\mathrm{T}})$.

B. Unit Circuit

We constructed unit circuit, i.e., a second-order CNN cell circuit, with two cell circuits. Fig. 4 shows a schematic of the unit circuit. The circuit dynamics of the unit circuit are given by the following:

$$C\dot{V}^1 = -\frac{V^1}{R} + \frac{I_b}{2}F_\mu(C^{1+,1}V^1 - C^{1-,2}V^2) \tag{19}$$

$$C\dot{V}^2 = -\frac{V^2}{R} + \frac{I_b}{2}F_\mu(C^{2+,1}V^1) \tag{20}$$

where V^1 and V^2 represent the voltages of the first and second cells, $C^{m\pm,n}$ the coupling capacitance, $(m, n = 1, 2)$. The first and second cells interact with each other via capacitive coupling. This circuit has a trivial equilibrium point, $(V^1, V^2) = (0,0)$. The stability of the equilibrium point depends on all of the physical parameters involved, which is mainly attained by adjusting capacitive couplings. When the circuit has only a trivial equilibrium point and is unstable, the circuit shows oscillatory behavior, a limit-cycle oscillation.

C. Network Circuits

We constructed an entire network circuit with four unit circuits, connected to each other via capacitive couplings. The network dynamics are given by the following:

$$C\dot{V}_{i,j}^1 = -\frac{V_{i,j}^1}{R} + \frac{I_b}{2}F_\mu\left(\sum_{k,l,n} C_{i,j;k,l}^{1+,n}V_{k,l}^n - \sum_{k,l,n} C_{i,j;k,l}^{1-,n}V_{k,l}^n\right) \tag{21}$$

$$C\dot{V}_{i,j}^2 = -\frac{V_{i,j}^2}{R} + \frac{I_b}{2}F_\mu\left(\sum_{k,l,n} C_{i,j;k,l}^{2+,n}V_{k,l}^n - \sum_{k,l,n} C_{i,j;k,l}^{2-,n}V_{k,l}^n\right) \tag{22}$$

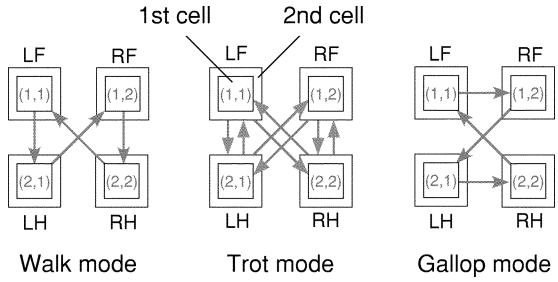

Fig. 5. Coupling configurations of network circuit for generating rhythmic patterns that correspond to walk, trot, and gallop mode operations.

where $V_{i,j}^1$ and $V_{i,j}^2$ represent the voltages of the first and second cells, $C_{i,j;k,l}^{m\pm,n}$ the coupling capacitance, (k,l) is a grid point in the neighborhood of unit (i,j). The total capacitance of each floating gate is given by

$$C_{\mathrm{T}} = C_{\mathrm{GD}} + C_{\mathrm{GS}} + C_{\mathrm{GB}} + \sum_{k,l,n} C_{i,j;k,l}^{m\pm,n} + C_{ctrl,i,j}^{m\pm} \tag{23}$$

where $C_{ctrl,i,j}^{m\pm}$ is the capacitance of each of the control gates, which was added to regulate the total capacitance of the floaring-gate and connected to grand potential.

Depending on its coupling configuration, the network circuit generates a different rhythmic pattern. Fig. 5 shows network configurations that generate rhythmic patterns corresponding to locomotion patterns of mammals, such as walk, trot and gallop. Here, the grid points (1, 1), (1, 2), (2, 1), and (2, 2) correspond to LF, RF, LH, and RH, respectively. It should be noted that the function of the network circuit considered here is cooperation between the limbs, i.e., interlimb coordination, described in Section II-A.

Both of the state variables in the circuit and the interaction between cells are expressed as voltages instead of currents. In particular, the interaction is implemented by the capacitive coupling. Consequently, we expect to reduce the total amount of the power consumption. Furthermore, the circuit can be expected operate precisely due to good matching accuracy of capacitances in silicon.

IV. Experimental Results

We designed and fabricated a CPG chip using a standard CMOS 1.5-μm process. Fig. 6 shows a photograph of the chip including four unit circuits without RC circuits. We constructed the RC circuits with off-chip capacitors and resistors so that we could set any time constant $\tau = RC$. The unit circuit consists of two cell circuits (Fig. 3). The design parameters of the cell circuit are listed in Table I. Each of MIFG MOS transistors in the unit circuit has ten input gates, each of which is $28\,\lambda \times 28\,\lambda$, (scaling parameter $\lambda = 0.8\,\mu$m). The input gates were mainly connected to pads, and partly to voltage nodes via on-chip connections.

A. Measured Results of Unit Circuit

We first confirmed oscillatory behavior of the unit circuit. We implemented capacitive coupling with interconnections on chip, and set coupling capacitances as follows:

$$C^{1+,1} = C^{1-,2} = 5C_i,\ C^{2+,1} = 3C_i \tag{24}$$

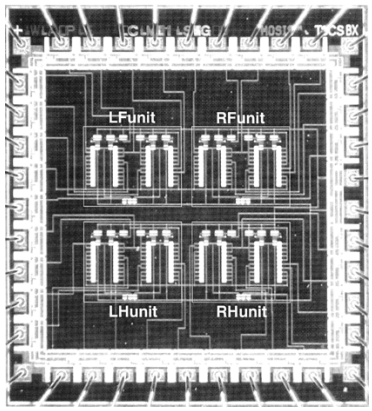

Fig. 6. Microphotograph of fabricated chip.

TABLE I
PARAMETERS OF UNIT CIRCUIT

	L (μm)	W (μm)
M1, M2, M3	8	48
M4, M5	8	24

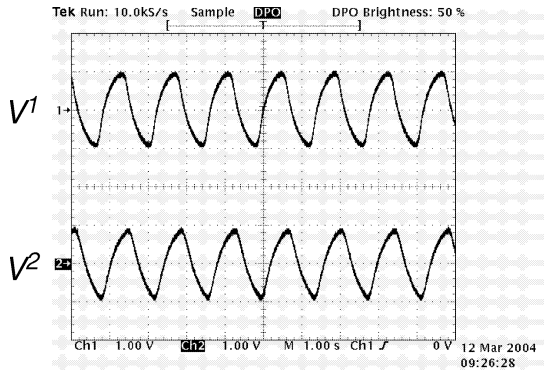

Fig. 7. Waveforms of measured voltages V^1 and V^2 in unit circuit.

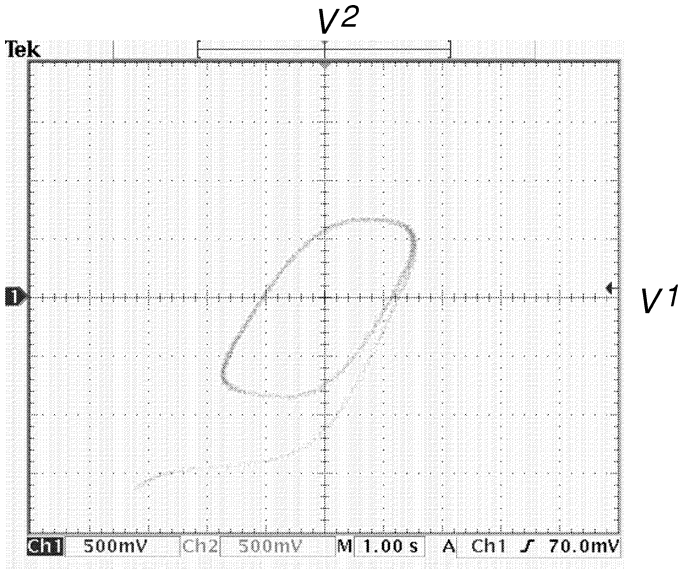

Fig. 8. Closed (V^1, V^2) phase-plane portrait of unit circuit, where both the initial voltages V^1 and V^2 were set at VSS.

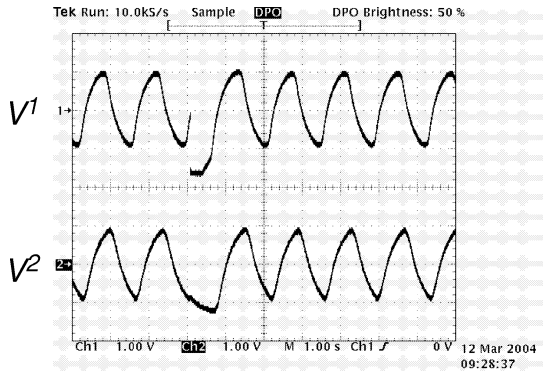

Fig. 9. Influence of disturbance in unit circuit, where we reset voltage V^1 at VSS suddenly. Despite such a strong disturbance, a steady-state of unit circuit were recovered promptly.

where C_i is the capacitance of each input gate, calculated at 0.29 pF. The total capacitance of floating-gate $C_{\rm T}$ was estimated at 3.2 pF. For purposes of setting the equilibrium voltages of the unit circuit at zero, we established the circuit parameters as follows: the capacitance $C = 100$ nF, the resistance $R = 3.3$ MΩ, the bias current $I_b = 1$ μA, and the supply voltages VDD $= 1.65$ V and VSS $= -1.65$ V. After we had removed initial floating-gate charges by illuminating the chip with ultraviolet (UV) light, we measured voltages V^1 and V^2 in the unit circuit under a noisy environment. We calculated the ratio between the maximum amplitude of the measured voltages and background noise, i.e, the signal-to-noise ratio (SNR), which was about 30 dB.

Fig. 7 shows the waveforms of voltages measured in the unit circuit. Both measured voltages V^1 and V^2 exhibit nonlinear oscillations. There exists a slightly delay between V^1 and V^2. Fig. 8 shows a closed (V^1, V^2) phase-plane portrait, where both the initial voltages V^1 and V^2 were set at VSS. We can observe a stable limit-cycle oscillation in the unit circuit. To see the stability of the unit circuit, we reset the voltage V^1 at VSS suddenly (Fig. 9). Despite such a strong disturbance, a staedy-state of the unit circuit were recovered promptly. This indicates that limit-cycle oscillations in the unit circuit are stable against unexpected disturbances.

B. Measured Results of Network Circuits

We then checked rhythmic patterns generated in network circuits. Using the coupling configurations shown in Fig. 5, we constructed network circuits by connecting unit circuits to each other via capacitive couplings. The self coupling capacitances of the unit circuits were set at:

$$C_{\rm LF}^{1+,1} = C_{\rm RF}^{1+,1} = C_{\rm LH}^{1+,1} = C_{\rm RH}^{1+,1} = 5C_i$$
$$C_{\rm LF}^{1-,2} = C_{\rm RF}^{1-,2} = C_{\rm LH}^{1-,2} = C_{\rm RH}^{1-,2} = 5C_i$$
$$C_{\rm LF}^{2+,1} = C_{\rm RF}^{2+,1} = C_{\rm LH}^{2+,1} = C_{\rm RH}^{2+,1} = 3C_i$$

where we replaced the grid points (1,1), (1,2), (2,1), and (2,2) with LF, RF, LH, and RH, respectively. We measured voltages $V_{i,j}^1$ in the network circuits under the same conditions as in the previous experiments. Fig. 10(a) and (b) show the waveforms of measured voltages in network circuits in walk and trot mode operation, respectively.

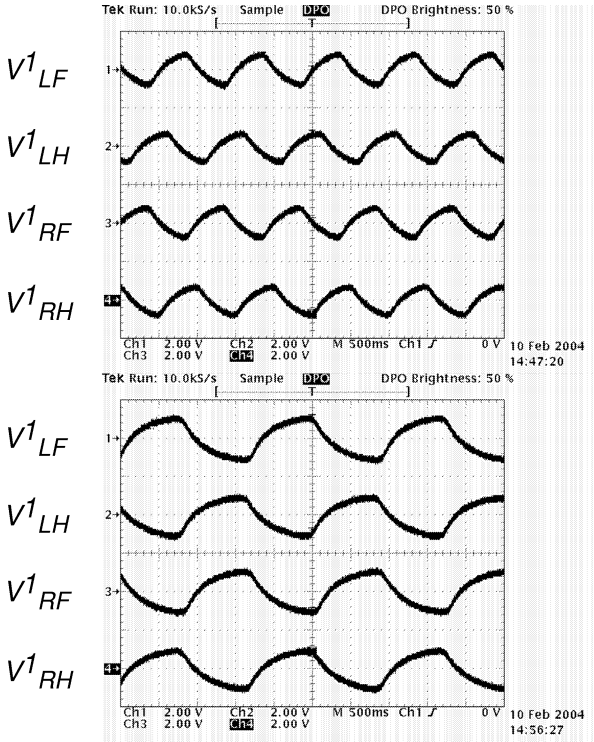

Fig. 10. Waveforms of measured voltage $V^1_{i,j}$ in network circuits. (a) Walk and (b) trot mode.

In the walk mode, the coupling capacitances between the unit circuits were set at:

$$C^{1-,1}_{\mathrm{LF;RH}} = C^{1-,1}_{\mathrm{RF;LH}} = C^{1-,1}_{\mathrm{LH;LF}} = C^{1-,1}_{\mathrm{RH;RF}} = C_i$$

and the others were set at 0 F.

In the trot mode, the coupling capacitances between the unit circuits were set at:

$$C^{1-,2}_{\mathrm{LF;RH}} = C^{1-,2}_{\mathrm{RF;LH}} = C^{1-,2}_{\mathrm{LH;RF}} = C^{1-,2}_{\mathrm{RH;LF}} = C_i$$
$$C^{2-,2}_{\mathrm{LF;LH}} = C^{2-,2}_{\mathrm{RF;RH}} = C^{2-,2}_{\mathrm{LH;LF}} = C^{2-,2}_{\mathrm{RH;RF}} = 2C_i$$

and the others were set at 0 F.

If we assume that $V^1_{1,1}$, $V^1_{1,2}$, $V^1_{2,1}$, and $V^1_{2,2}$ create target joint angles θ_{LF}, θ_{RF}, θ_{LH}, and θ_{RF} for a quadruped robot, then the waveforms of measured voltages can be considered as the locomotion patterns of mammals depicted in Fig. 1. Fig. 11(a) and (b) show the desired phase relationships between the joint angles for interlimb coordination in quadruped robot locomotion.

In the present experiments, we only considered two coupling configurations that corresponded to the walk and the trot modes, because the gallop mode was topologically equivalent to the walk mode. Had we considered another coupling configuration, a different rhythmic pattern would have been generated.

By approximately regarding the waveforms of measured voltages as sinusoidal waves, we calculated how much current was in the chip during operation as follows:

$$\text{power consumption} = (\mathrm{VDD} - \mathrm{VSS}) \cdot \frac{3}{2} I_b \times N$$

where N represents the number of cell circuits. We also assumed the average current through M1 in Fig. 2 was $I_b/2$. In a steady state, the amount of the electrical power was 39.6 μW.

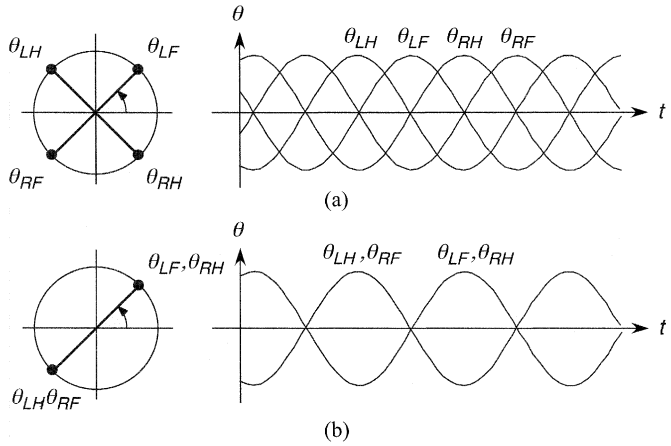

Fig. 11. Desired phase relationships for controlling in quadruped robot locomotion. (a) Walk and (b) trot mode.

These results indicate that our CPG chip generates stable rhythmic patterns that correspond to the locomotion patterns in mammals even under a noisy environment, and achieves low power consumption during operation. Such characteristics of the CPG chip are suitable for controlling locomotion in a quadruped walking robot in real situations.

V. Discussion

Let us discuss the advantages and disadvantages of our approach in analog circuit implementation of a locomotion controller based on the CPG framework.

A. Related Works

First, let us compare between the current and related works with analog circuit implementation of CPGs, discussed in previous works [13]–[19]. In the earliest of these, Ryckebusch *et al.* implemented small CPG networks as analog VLSI systems [13]. Their circuits are constructed with simple neuron circuits, i.e., the Axon–Hillock integrate and fire neuron (IFN) circuits [33]. Althrough their circuits look simple, they capture some of the essential features of the function of CPGs, such as synaptic interactions and temporal delays [13]. Still and Tilden implemented an analog CPG circuit based on the Nv neuron circuit [14]. Their circuit, while quite simple, also contains such essential features, and succeeded in controlling a quadruped walking robot [14]. Patel *et al.* designed an analog CPG chip, based on the Morris–Lecar neuron circuit, faithfully modeled after a biological neuron [16]. Lewis and his collaborators developed analog CPG chips with IFN circuits to control walking robots [17], [18]. Their chips has sensory feedback loops that help them to adapt to a given situation.

Although these circuits have advantages, as previously discussed, it is difficult to determine circuit parameters to generate the desired rhythmic pattern due to deviations in devices and the strong nonlinearity in the circuits. Recently, Still introduced a learning algorithm to achieve the rhythmic pattern they required into their chip, but it was necessary to control several bias voltages [15].

In contrast, our approach to analog circuit implementation of CPGs is very easy in terms of determining circuit parameters. We considered a class of CNNs, i.e., a modified CNN as a CPG model. The nonlinearity characteristics of our model can be easily obtained by using a differential pair, and therefore we can directly implement it as an analog CPG chip. Thus, we can easily determine the circuit parameters based on the results obtained from the numerical analysis.

Previously proposed CNN-based CPG controllers have been implemented on silicon chips [31], [32]. Branciforte *et al.* proposed an analog chip that operates through interaction of current [31]. Their chip is constructed with many current amplifiers, and then it has good programability. However, it is difficult to operate stably without tuning bias currents because of the irregularity of currents through the current amplifiers. Arena *et al.* proposed a hybrid VLSI chip, based on the operational amplifier implementation of CNN cells [32] and the switched-capacitor technique [21]. Their chip has an advantage in controlling the operation speed. However, cells are interacting through currents in these chips, and thus these chips have problems in terms of current mismatch and power consumption. Keeping such problems in mind, we have represented both state variables and the interaction between cells, i.e., signal, as voltages instead of currents. In particular, the interactions have been implemented via capacitive couplings. Consequently, we have achieved low power consumption during operation. The power consumption in a chip is usually smaller than in actuators. Nevertheless, low power consumption is critical in long-term operations in a micro locomotion robot. In addition, interactions are highly accurate because of good matching accuracy of capacitances in silicon, and thus our chip operate precisely.

In our previous work, we designed an analog CPG circuit that consists of the Amari–Hopfield neuron model [19]. Our previous works is based on the neural network model proposed by Nagashino *et al.* Their model is a special case of the continuous-time recurrent neural network (CTRNN) [10]. The interaction terms in our previous circuit are implemented with current mirrors. Thus current mismatch is a critical issue to attein precise operation. In contrast, our present circuit is designed as an analog voltage-mode circuit, resulting in precise operation.

B. Parameter Setup

We can determine the circuit parameters based on the results of numerical analysis and circuit simulations. In practice, we analyzed the equations given by (7)–(8), and then estimated the coupling capacitances. After circuit simulations using SPICE macro model for floating-gate devices (cf. [37]), we determined the coupling configuration for a practical circuit. However, we need to note that the coupling configuration has been partly determined by the layout of the fabricated chip. This means that the input-gates are mainly connected to pads, and can be reconnected to any voltage node $V^n_{i,j}$. Thus, we can change the operation mode by switching the voltage nodes connected to the input-gates.

To set the time constant required to control locomotion in a practical robot, we used off-chip capacitors and resistors. If the time constant required for operational speed is nearly equal to animals such as horses, we need a large capacitance or large resistance, which is difficult to obtain on silicon chips.

C. Practical Problems for Precise Operation

Our CPG chip is assumed to operate in the weak inversion region to reduce current consumption. However, it can also operate in both moderate and strong inversion regions since the transfer characteristics of the differential pair are qualitative the same in all operation regions. If the bias current is increased, the current gain of the differential pair is decreased. Consequently, the amplitude of the waveforms of voltages $V^n_{i,j}$ are increased. We should set the supply voltages, VDD and VSS, so that they are greater than the expected maximum amplitude of the waveforms of the voltages $V^n_{i,j}$.

Mismatch in a pair of transistors can seriously affect the offset voltage of a differential pair and the current transfer ratio of a current mirror. Such mismatch can be reduced by enlarging the size of transistors. The deviations in leak current of MOS transistors in silicon are a function of gate width W and gate length L [21]. If we make transistors larger, the deviations can be reduced. The value of leak current is also depends on the aspect ratio of W/L, and thus excessively large transistors will degrade the performance of our chip. We optimized the parameters as listed in Table I.

The main practical problems with our chip is the initial floating-gate charge that also affects the offset voltage of the differential pair. If we remove the floating-gate charge by illuminating the chip with UV light as used in Section IV, this problem would be improved.

VI. Summary

We have presented analog CMOS implementation of a CNN-based CPG model for locomotion control in a quadruped walking robot. We have introduced an affine transformation of CNN equations, and have designed it as an analog CMOS circuit using MIFG MOS transistors, aimed at voltage-mode operation. We have fabricated an experimental chip using a standard CMOS process. Through several experiments on the fabricated chip, we have shown that our chip generates stable rhythmic patterns that correspond to the typical locomotion patterns of mammals even if under a noisy environment, and low power consumption is realized. These characteristics are sufficient for a CPG to do the interlimb coordination required in quadruped robot locomotion.

Following the present research, we are going to develop a practical locomotion controller for a quadruped walking robot. The present chip has not been fully implemented as a locomotion controller. We have only implemented the second function of CPG described in Section II-A, i.e., interlimb coordination. The first functions of CPG, i.e., controlling the trajectory of individual limbs, can easily be implemented by feedforward connections of unit circuits in the chip. However, it is difficult to determine the coupling capacitances and time constant because these depend on the physical parameters of a practical robot, such as the length of joints and the mass of limbs. Furthermore, the integration of sensory feedback between the state of the limb and the state of the unit circuit in the chip is required for stable

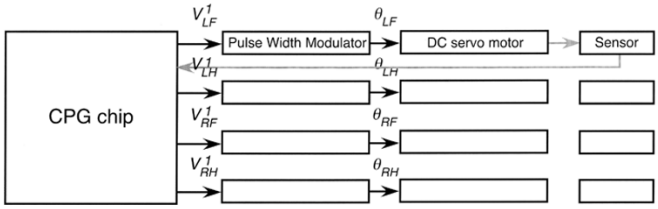

Fig. 12. Block diagrams of complete locomotion controller.

locomotion. If a sensory feedback signal, such as a joint angle, is directly fed into an input-gate as voltage, and mutual entrainment between the limb and unit circuit can occur, this result will in adaptation to an unexpected disturbance. Such entrainment can be confirmed through numerical analysis using (7)–(8) described in Section II-B. For future developments, we have considered a complete locomotion controller, as depicted in Fig. 12. We assume that the output voltages of the chip give target joint angles to dc servo motors that drive joints of a quadruped robot using pulse wide modulators, and sensory signals are directly fed into the chip. Developing and evaluating of a locomotion controller in a practical robot are further considerations.

REFERENCES

[1] A. H. Cohen, "Control principles for locomotion – Looking toward biology," in *Proc. 2nd Int. Symp. Adaptive Motion of Animals and Machines*, 2003.

[2] F. Delcomyn, "Neural basis of rhythmic behavior in animals," *Science*, vol. 210, pp. 492–498, 1980.

[3] *The Handbook of Brain Theory and Networks*, 2nd ed., M. Arbib, Ed., MIT Press, Cambridge, MA, 2002.

[4] F. Delcomyn, *Foundations of Neurobiology*. New York: Freeman, 1997.

[5] A. I. Dagg, "Gait in mammals," *Mammal Rev.*, vol. 3, pp. 135–154, 1973.

[6] H. R. Wilson and J. D. Cowan, "Excitatory and inhibitory interactions in localized populations of model neurons," *Biophys. J.*, vol. 12, pp. 1–24, 1972.

[7] K. Matsuoka, "Mechanism of frequency and pattern control in the neural rhythm generators," *Biol. Cybern.*, vol. 56, pp. 345–353, 1987.

[8] G. Taga, Y. Yamaguchi, and H. Shimizu, "Self-organized control of bipedal locomotion by neural oscillators in unpredictable environment," *Biol. Cybern.*, vol. 65, pp. 147–159, 1991.

[9] H. Nagashino, Y. Nomura, and Y. Kinouchi, "Generation and transitions of phase-locked oscillations in coupled neural oscillators," in *Proc. 40h SICE Annual Conf.*, Nagoya, Japan, 2001.

[10] R. D. Beer, H. J. Chiel, and J. C. Gallagher, "Evolution and analysis of model CPGs for walking II: General principles and individual variability," *J. Comput. Neurosci.*, vol. 7, pp. 119–147, 1999.

[11] H. Kimura, Y. Fukuoka, and K. Konaga, "Adaptive dynamic walking of a quadruped robot by using neural system model," *Adv. Robot.*, vol. 15, no. 8, pp. 859–876, 2001.

[12] A. Billard and A. J. Ijspeert, "Biologically inspired neural controllers for motor control in a quadruped walking robot," in *Proc. IEEE-INNS Int. Joint Conf. on Neural Networks*, Italy, Jul. 2000.

[13] S. Ryckebusch, J. M. Bower, and C. A. Mead, "Modeling small oscillating biological networks in analog VLSI," *Adv. Neural Information Processing Syst.*, vol. 1, pp. 384–393, 1989.

[14] S. Still and M. W. Tilden, "Controller for a four legged walking machine," in *Neuromorphic Systems Engineering Silicon from Neurobiology*, L. S. Smith and A. Hamilton, Eds. Singapore: World Scientific, 1998, pp. 138–148.

[15] S. Still, B. Scholkopf, K. Hepp, and R. J. Douglas, "Four-legged walking gait control using a neuromorphic chip interfaced to a support vector learning algorithm," *Adv. Neural Inf. Process. Syst.*, vol. 13, pp. 741–747, 2001.

[16] G. Patel, J. Holleman, and S. DeWeerth, "Analog VLSI model of intersegmental cordination with nearest-neighbor coupling," *Adv. Neural Inf. Process. Syst.*, vol. 10, pp. 710–725, 1998.

[17] M. A. Lewis, M. J. Harttmann, R. Etienne-Cummings, and A. H. Cohen, "Control of a robot leg with an adaptive aVLSI CPG chip," *Neurocomp.*, vol. 38–40, pp. 1409–1421, 2001.

[18] F. Tenore, R. Etienne-Cummings, and M. A. Lewis, "A programmable array of silicon neurons for the control of legged locomotion," in *Proc. Int. Symp. Circuits and Systems*, Vancouver, QC, Canada, 2004.

[19] K. Nakada, T. Asai, and Y. Amemiya, "An analog central pattern generator for interlimb coordination in quadruped locomotion," *IEEE Trans. Neural Netw.*, vol. 14, no. 5, pp. 1356–1365, Oct. 2003.

[20] M. Branciforte, G. Di Bernardo, F. Doddo, and L. Occhipinti, "Reaction-diffusion CNN design for a new class of biologically-inspired processors in artificial locomotion applications," in *Proc. 7th Int. Conf. Microelectronics for Neural, Fuzzy and Bio-Inspired Systems*, Granada, Spain, 1999, pp. 69–77.

[21] P. Arena, S. Castorina, L. Fortuna, M. Frasca, and M. Ruta, "A CNN chip for robot locomotion control," in *Proc. IEEE Int. Symp. Circuits Systems*, vol. 3, May 2003, pp. 510–513.

[22] L. O. Chua and L. Yang, "Cellular neural networks: Theory," *IEEE Trans. Circuits Syst. I, Fundam. Theory Appl.*, vol. 35, no. 10, pp. 1257–1272, Oct. 1988.

[23] ——, "Cellular neural networks: Application," *IEEE Trans. Circuits Syst. I, Fundam. Theory Appl.*, vol. 35, no. 10, pp. 1273–1290, Oct. 1988.

[24] L. O. Chua and T. Roska, "The CNN paradigm," *IEEE Trans. Circuits Syst. I, Fundam. Theory Appl.*, vol. 40, no. 3, pp. 147–156, Mar. 1993.

[25] L. O. Chua, M. Hasler, G. S. Moschytz, and J. Neirynck, "Autonomous cellular neural networks: A unified paradigm for pattern formation and active wave propagation," *IEEE Trans. Circuits Syst. I, Fundam. Theory Appl.*, vol. 42, no. 10, pp. 559–557, Oct. 1995.

[26] L. Pivka, "Autowaves and spatio-temporal chaos in CNNs. I-II," *IEEE Trans. Circuits Syst. I, Fundam. Theory Appl.*, vol. 42, no. 10, pp. 638–664, Oct. 1995.

[27] L. Goras, L. O. Chua, and D. M. W. Leenaerts, "Turing patterns in CNNs. I-III. Once over lightly," *IEEE Trans. Circuits Syst. I, Fundam. Theory Appl.*, vol. 42, no. 10, pp. 602–637, Oct. 1995.

[28] P. Thiran, K. R. Crounse, L. O. Chua, and M. Hasler, "Pattern formation properties of autonomous cellular neural networks," *IEEE Trans. Circuits Syst. I, Fundam. Theory Appl.*, vol. 42, no. 10, pp. 757–774, Oct. 1995.

[29] T. Roska, L. O. Chua, D. Wolf, T. Kozek, R. Tetzlaff, and F. Puffer, "Simulating nonlinear waves and partial differential equations via CNN – Part I: Basic techniques," *IEEE Trans. Circuits Syst. I, Fundam. Theory Appl.*, vol. 42, no. 10, pp. 807–815, Oct. 1995.

[30] P. Arena, S. Baglio, L. Fortuna, and G. Manganaro, "Self-organization in a two layer CNN," *IEEE Trans. Circuits Syst. I, Fundam. Theory Appl.*, vol. 45, no. 2, pp. 157–162, Feb. 1998.

[31] P. Arena, L. Fortuna, and M. Branciforte, "Reaction-diffusion CNN algorithms to generate and control artificial locomotion," *IEEE Trans. Circuits Syst. I, Fundam. Theory Appl.*, vol. 46, no. 2, pp. 253–260, Feb. 1999.

[32] P. Arena, "Realization of a reaction-diffusion CNN algorithms for locomotion control in an hexapod robot," *J. VLSI Signal Processing*, vol. 23, no. 2, pp. 267–280, 1999.

[33] C. A. Mead, *Analog VLSI and Neural Systems*. Reading, MA: Addison-Wesley, 1989.

[34] M. Isami and T. Fiez, Eds., *Analog VLSI: Signal and Information Processing*. New York: McGraw-Hill, 1993.

[35] T. Shibata and T. Ohmi, "A functional MOS transistor featuring gate level weighted sum and threshold operations," *IEEE, Trans. Electron. Dev.*, vol. 39, no. 6, pp. 1444–1445, 1990.

[36] B. A. Minch, C. Diorio, P. Hasler, and C. A. Mead, "Translinear circuits using subthreshold floating-gate MOS transistors," *Anal. Int. Circuits Signal Process.*, vol. 9, no. 2, pp. 167–179, 1998.

[37] A. F. Mndragon-Torres, E. Sanchez-Sinenco, and K. R. Narayanan, "Floating-gate analog implementation of the additive soft-input soft-output decoding algorithm," *IEEE Trans. Circuits Syst. I, Fundam. Theory Appl.*, vol. 50, no. 10, pp. 1256–69, Oct. 2003.

[38] L. Vancaillie, F. Silveira, B. Linares-Barranco, T. Serrano-Gotarredona, and D. Flandre, "MOSFET mismatch in weak/moderate inversion: Model needs and implications for analog design," in *Proc. 2003 Eur. Solid-State Circuits Conf.*, Sep. 2003, pp. 671–674.

Kazuki Nakada (S'02–A'02) received the B.S. degree in mathematics and M.E. degree in systems and information engineering from Hokkaido University, Sapporo, Japan, in 1999 and 2002, respectively. He is currently working toward the Dr. Eng. Degree in the Department of Electrical Engineering at the same university.

His current research interests include biologically inspired robotics and neuromorphic systems.

Tetsuya Asai (M'01) received the B.E. and M.E. degrees in electrical engineering from Tokai University, Kanagawa, Japan, in 1993 and 1996, respectively, and the Dr. Eng. degree in electrical and electronic engineering from the Toyohashi University of Technology, Aichi, Japan, in 1999.

He is an Associate Professor in the Department of Electrical Engineering, Hokkaido University, Sapporo, Japan. His current research interests include sensory information processing in neural networks as well as design and applications of neuromorphic very large-scale integrations and the reaction-diffusion chip.

Yoshihito Amemiya received the B.E., M.E., and Dr.Eng. degrees from the Tokyo Institute of Technology, Tokyo, Japan, in 1970, 1972, and 1975, respectively.

From 1975 to 1993, he was with NTT LSI Laboratory, Atsugi, Japan. Since 1993, he has been a Professor in the Department of Electrical Engineering, Hokkaido University, Sapporo, Japan. His research interests are in electronic circuits, large-scale integration (LSI) circuits, functional devices based on nonlinear analog computation, logic systems using single-electron circuits, and information processing devices using quantum-effect nanostructures.